Evaluation of a spectrally resolved scattering microscope

Michael Schmitz,* Thomas Rothe, and Alwin Kienle

Institut für Lasertechnologien in der Medizin und Meßtechnik, 89081 Ulm, Germany

**michael.schmitz@ilm.uni-ulm.de*

Abstract: A scattering microscope was developed to investigate single cells and biological microstructures by light scattering measurements. The spectrally resolved part of the setup and its validation are shown in detail. The analysis of light scattered by homogenous polystyrene spheres allows the determination of their diameters using Mie theory. The diameters of 150 single polystyrene spheres were determined by the spectrally resolved scattering microscope. In comparison, the same polystyrene suspension stock was investigated by a collimated transmission setup. Mean diameters and standard deviations of the size distribution were evaluated by both methods with a statistical error of less than 1 nm. The systematic errors of both devices are in agreement within the measurement accuracy.

OCIS codes: (180.0180) Microscopy; (290.1350) Back scattering; (290.2200) Extinction, (290.4020) Mie theory; (290.5850) Scattering, particles; (300.6550) Spectroscopy, visible.

References and links

1. A. Amelink, M. P. L. Bard, S. A. Burgers, and H. J. C. M. Sterenborg, "Single-scattering spectroscopy for the endoscopic analysis of particle size in superficial layers of turbid media," Appl. Opt. **42**, 4095–4101 (2003).
2. Y. Liu, X. Li, Y. L. Kim, and V. Backman, "Elastic backscattering spectroscopic microscopy," Opt. Lett. **30**, 2445–2447 (2005).
3. F. K. Forster, A. Kienle, R. Michels, and R. Hibst, "Phase function measurements on nonspherical scatterers using a two-axis goniometer," J. Biomed. Opt. **11**, 024018 (2006).
4. M. J. Berg, S. C. Hill, G. Videen, and K. P. Gurton, "Spatial filtering technique to image and measure two-dimensional near-forward scattering from single particles," Opt. Express **18**, 9486–9495 (2010).
5. P. Albella, J. M. Saiz, J. M. Sanz, F. González, and F. Moreno, "Nanoscopic surface inspection by analyzing the linear polarization degree of the scattered light," Opt. Lett. **34**, 1906–1908 (2009).
6. M. S. Patterson, B. Chance, and B. C. Wilson, "Time resolved reflectance and transmittance for the non-invasive measurement of tissue optical properties," Appl. Opt. **28**, 2331–2336 (1989).
7. T. Namita, Y. Kato, and K. Shimizu, "CT imaging of diffuse medium by time-resolved measurement of back-scattered light," Appl. Opt. **48**, D208–D217 (2009).
8. J. R. Mourant, I. J. Bigio, D. A. Jack, T. M. Johnson, and H. D. Miller, "Measuring absorption coefficients in small volumes of highly scattering media: source-detector separations for which path lengths do not depend on scattering properties," Appl. Opt. **36**, 5655–5661 (1997).
9. A. Kienle, C. D'Andrea, F. Foschum, P. Taroni, and A. Pifferi, "Light propagation in dry and wet softwood," Opt. Express **16**, 9895–9906 (2008).
10. V. Backman, R. Gurjar, K. Badizadegan, I. Itzkan, R. Dasari, L. Perelman, and M. Feld, "Polarized light scattering spectroscopy for quantitative measurement of epithelial cellular structures in situ," IEEE J. Sel. Top. Quantum Electron. **5**, 1019–1026 (1999).
11. J. Allen, Y. Liu, Y. L. Kim, V. M. Turzhitsky, V. Backman, and G. A. Ameer, "Spectroscopic translation of cell-material interactions," Biomaterials **28**, 162–174 (2007).
12. L. B. Lovat, K. Johnson, G. D. Mackenzie, B. R. Clark, M. R. Novelli, S. Davies, M. O'Donovan, C. Selvasekar, S. M. Thorpe, D. Pickard, R. Fitzgerald, T. Fearn, I. Bigio, and S. G. Bown, "Elastic scattering spectroscopy accurately detects high grade dysplasia and cancer in Barrett's oesophagus," Gut **55**, 1078–1083 (2006).

#150625 - $15.00 USD Received 6 Jul 2011; revised 2 Aug 2011; accepted 16 Aug 2011; published 23 Aug 2011

13. A. K. Popp, M. T. Valentine, P. D. Kaplan, and D. A. Weitz, "Microscopic origin of light scattering in tissue," Appl. Opt. **42**, 2871–2880 (2003).
14. K. Rebner, M. Schmitz, B. Boldrini, A. Kienle, D. Oelkrug, and R. W. Kessler, "Dark-field scattering microscopy for spectral characterization of polystyrene aggregates," Opt. Express **18**, 3116–3127 (2010).
15. H. Fang, L. Qiu, E. Vitkin, M. M. Zaman, C. Andersson, S. Salahuddin, L. M. Kimerer, P. B. Cipolloni, M. D. Modell, B. S. Turner, S. E. Keates, I. Bigio, I. Itzkan, S. D. Freedman, R. Bansil, E. B. Hanlon, and L. T. Perelman, "Confocal light absorption and scattering spectroscopic microscopy," Appl. Opt. **46**, 1760–1769 (2007).
16. P. Huang, M. Hunter, and I. Georgakoudi, "Confocal light scattering spectroscopic imaging system for in situ tissue characterization," Appl. Opt. **48**, 2595–2599 (2009).
17. W. J. Cottrell, J. D. Wilson, and T. H. Foster, "Microscope enabling multimodality imaging, angle-resolved scattering, and scattering spectroscopy," Opt. Lett. **32**, 2348–2350 (2007).
18. Z. J. Smith and A. J. Berger, "Validation of an integrated Raman- and angular-scattering microscopy system on heterogeneous bead mixtures and single human immune cells," Appl. Opt. **48**, D109–D120 (2009).
19. R. Arimoto and J. Murray, "Orientation-dependent visibility of long thin objects in polarization-based microscopy," Biophys. J. **70**, 2969–2980 (1996).
20. H. K. Roy, Y. Liu, R. K. Wali, Y. L. Kim, A. K. Kromine, M. J. Goldberg, and V. Backman, "Four-dimensional elastic light-scattering fingerprints as preneoplastic markers in the rat model of colon carcinogenesis," Gastroenterology **126**, 1071–1081 (2004).
21. T. Rothe, M. Schmitz, and A. Kienle, "Angular resolved scattering microscopy," in "Advanced Microscopy Techniques II," (SPIE, 2011), 808613.
22. L. T. Perelman, V. Backman, M. Wallace, G. Zonios, R. Manoharan, A. Nusrat, S. Shields, M. Seiler, C. Lima, T. Hamano, I. Itzkan, J. Van Dam, J. M. Crawford, and M. S. Feld, "Observation of periodic fine structure in reflectance from biological tissue: A new technique for measuring nuclear size distribution," Phys. Rev. Lett. **80**, 627–630 (1998).
23. H. Fang, M. Ollero, E. Vitkin, L. Kimerer, P. Cipolloni, M. Zaman, S. Freedman, I. Bigio, I. Itzkan, E. Hanlon, and L. Perelman, "Noninvasive sizing of subcellular organelles with light scattering spectroscopy," IEEE J Sel Top Quantum Electron **9**, 267–276 (2003).
24. A. Kienle and R. Hibst, "Light guiding in biological tissue due to scattering," Phys. Rev. Lett. **97**, 018104 (2006).
25. A. Kienle, C. Wetzel, A. Bassi, D. Comelli, P. Taroni, and A. Pifferi, "Determination of the optical properties of anisotropic biological media using an isotropic diffusion model," J. Biomed. Opt. **12**, 014026 (2007).
26. G. Mie, "Beiträge zur Optik trüber Medien, speziell kolloidaler Metallösungen," Ann. Phys. **330**, 377–445 (1908).
27. C. F. Bohren and D. R. Huffman, *Absorption and Scattering of Light by Small Particles* (Wiley, 1983).
28. R. Michels, "Verständnis des mikroskopischen Ursprungs der Lichtstreuung in biologischem Gewebe," doctoral dissertation, Ulm University (2010).
29. C. Tribastone and W. Peck, "Designing plastic optics: New applications emerging for optical glass substitutes," in *The Photonics Design and Applications Handbook*, (Laurin Publishing, 1998), pp. H426–H433.
30. M. Schmitz, T. Rothe, and A. Kienle, "Comparison between spectral resolved scattering microscopy and collimated transmission measurements," in "Advanced Microscopy Techniques II," (SPIE, 2011), 808614.
31. M. Daimon and A. Masumura, "Measurement of the refractive index of distilled water from the near-infrared region to the ultraviolet region," Appl. Opt. **46**, 3811–3820 (2007).
32. X. Ma, J. Q. Lu, R. S. Brock, K. M. Jacobs, P. Yang, and X.-H. Hu, "Determination of complex refractive index of polystyrene microspheres from 370 to 1610 nm," Phys. Med. Biol. **48**, 4165–4172 (2003).
33. E. Collett, "Mueller-stokes matrix formulation of Fresnel's equations," Am. J. Phys. **39**, 517–528 (1971).
34. M. Schmitz, R. Michels, and A. Kienle, "Darkfield scattering spectroscopic microscopy evaluation using polystyrene beads," in "Clinical and Biomedical Spectroscopy," (SPIE, 2009), 73681W.
35. A. D. Ward, M. Zhang, and O. Hunt, "Broadband Mie scattering from optically levitated aerosol droplets using a white LED," Opt. Express **16**, 16390–16403 (2008).
36. A. Graßmann and F. Peters, "Size measurement of very small spherical particles by Mie scattering imaging (MSI)," Part. Part. Syst. Character. **21**, 379–389 (2004).
37. C. S. Mulvey, C. A. Sherwood, and I. J. Bigio, "Wavelength-dependent backscattering measurements for quantitative real-time monitoring of apoptosis in living cells," J. Biomed. Opt. **14**, 064013 (2009).

1. Introduction

Scattered light is often an annoying phenomenon in nature, whether it is fog outdoors or unwanted stray light inside the optics laboratory. Nevertheless, many conclusions on the structure, the size or the optical properties of a medium can be drawn by the analysis of scattered light. The scattering patterns can be observed spectrally resolved [1, 2], angular resolved [3, 4], polarization dependent [5], time resolved [6, 7] or spatially resolved [8, 9]. Moreover, various

#150625 - $15.00 USD Received 6 Jul 2011; revised 2 Aug 2011; accepted 16 Aug 2011; published 23 Aug 2011

publications of different combinations of these methods do exist [10, 11]. Light scattering measurements are non-invasive, therefore they are adequate for the investigation and diagnosis of biological tissue [12]. The contrast is given only by the scattering, so the technique is marker-free and no further enhancement is necessary. Microscopic setups are essential for the study of single cells [13] and chromosomes [14]. Experiments have been made with confocal microscopes [15, 16], brightfield microscopes [17], darkfield microscopes [18] or evanescent illumination [19], just to name a few different methods.

In this contribution a scattering microscope is presented that combines spectroscopic and angular resolved measurements, similar to the setup presented by Cottrell et al. [17]. But in contrast to this, the here shown setup includes several relevant differences. First of all, the presented microscope works on the basis of a reflected darkfield illumination. This is advantageous for the observation of thicker or strongly absorbing samples. Moreover, in case of Mie scattering, the spectral and angular patterns of the backward scattered light contain more information. In addition, Cottrell et al., as well as e.g. Smith and Berger [18], are using an illumination that is rotationally symmetric to the optical axis. On the contrary, the here shown scattering microscope is using an unidirectional illumination beam. Therefore the geometrical orientation of a non-spherical sample and the direction of illumination can be rotated against each other, which increases the versatility of the measurements. Further, in comparison to Cottrell's setup [17] or the 4D-ELF setup published by Roy et al. [20], the range of detected scattering angles is enlarged in our setup (from 93° to 157°).

This paper focuses on the spectrally resolved analysis of elastically scattered light. Further information about the angular resolved measurements performed by the here shown scattering microscope can be found in Rothe et al. [21].

Before starting studies on biological cells, a new setup has to be evaluated by well-known samples. Biological tissue is a complex medium, as it often contains multiple layers with miscellaneous structures having different scattering and absorption coefficients. Inner structures as cell cores and filaments can be approximated by spheres [22, 23], cylinders [24] or mixtures of these [25]. Light scattered by a homogenous sphere can be described analytically by Mie theory, which is a solution of Maxwell's equations [26]. Additionally, analytical solutions exist for an infinite cylinder [27].

Therefore, spheres and cylinders are an ideal reference sample for single scatterers. For the experiment, spherical microparticles are available in various sizes and materials. In many contributions, e.g. [2, 17], the determined sphere diameters are compared with the manufacturer values, which are commonly given in the form of a Gaussian size distribution. Thus, for the precise determination of systematic errors, the measurement of one or a few single spheres is insufficient. Here, polystyrene beads in suspension with a nominal mean diameter $\nu_n = 4.21\,\mu\text{m}$ and standard deviation $\sigma_n = 0.07\,\mu\text{m}$ were first analyzed by a well-approved collimated transmission setup [28]. Then, 150 single beads from the same stock were evaluated separately by the spectrally resolved scattering microscope. The agreement of both methods was verified by comparing the mean diameter ν and the standard deviation σ of the evaluated particle size distributions. By this approach, the statistical errors are reduced which enables a very precise measurement of systematic errors between both setups. In this case, systematic errors of less than 1 nm can be detected without the need of any complex or expensive setup as e.g. an electron microscope.

#150625 - $15.00 USD Received 6 Jul 2011; revised 2 Aug 2011; accepted 16 Aug 2011; published 23 Aug 2011

2. Theory

The here shown spectroscopic experiments are based on elastic light scattering by single, homogenous, spherical particles. Therefore, Mie theory provides an exact analytical solution. It is valid for any ratio of particle size to wavelength. In contrast to this, Rayleigh scattering or Fraunhofer diffraction are only reasonable approximations if particles are small or large compared to the wavelength λ, respectively. Input parameters for the Mie calculations are the diameter of the sphere D, the wavelength of the electromagnetic wave λ and the refractive indices of the sphere n_s [29, 30] and the medium surrounding it n_m [31]. Moreover, the imaginary part of the refractive indices has to be taken into account. However, the absorption of polystyrene is very low in the visible regime [32], thus it is neglected. Output parameters are the phase function p and the scattering cross section C_s. The phase function p is proportional to the amount of scattered light in a unit solid angle of a specific direction. Whereas the scattering cross section C_s is proportional to the likelihood of interaction between particle and plane electromagnetic wave. The theory of both experimental methods is further described in the following two subsections.

2.1. Particles in suspension measured by the collimated transmission setup

The extinction coefficient $\mu_{ext}(\lambda)$ can be measured by the collimated transmission setup. In the case of polystyrene bead suspensions the absorption coefficient $\mu_a(\lambda)$ can be neglected. Thus, the extinction coefficient $\mu_{ext}(\lambda)$ is equal to the scattering coefficient $\mu_s(\lambda)$. For a monodisperse suspension of spheres, the scattering coefficient is given by

$$\mu_s(\lambda) = \frac{f_V C_s(\lambda)}{V} \tag{1}$$

with the scattering cross section $C_s(\lambda)$, the volume concentration f_V and the sphere volume V. Thus, for non-absorbing spheres ($\mu_a = 0$) with a Gaussian probability distribution $g(D)$ of diameter D the extinction coefficient is

$$\mu_{ext,T}(\lambda, g(D)) = \mu_s + \mu_a = f_V \int_0^\infty \frac{g(D) C_s(\lambda, D)}{V(D)} \, \mathrm{d}D. \tag{2}$$

2.2. Single particles measured by the spectrally resolved scattering microscope

The following steps describe the theory of the spectrally resolved scattering microscope. The calculation of the theoretical spectra is performed by Mueller matrices. The scattering matrix $\mathbf{M}$ is calculated by Mie theory

$$\mathbf{M} = \frac{1}{k^2 r^2} \begin{pmatrix} S_{11} & S_{12} & 0 & 0 \\ S_{12} & S_{11} & 0 & 0 \\ 0 & 0 & S_{33} & S_{34} \\ 0 & 0 & -S_{34} & S_{33} \end{pmatrix} \tag{3}$$

with the wave number k and the distance to the detector r. Its elements S_{ij} are explained in Bohren and Huffman [27]. They have to be calculated for varying scattering angles Θ, sphere diameters D and wavelengths λ. The scattering angle Θ is given by the normalized wave vectors of the incident light $\vec{k}_i$ and of the scattered light $\vec{k}_s$,

$$\Theta = \arccos(\vec{k}_i \cdot \vec{k}_s) \tag{4}$$

with

$$\vec{k}_i = \begin{pmatrix} \sin\vartheta_i \\ 0 \\ \cos\vartheta_i \end{pmatrix}, \quad \vec{k}_s = \begin{pmatrix} \sin\vartheta\cos\varphi \\ \sin\vartheta\sin\varphi \\ \cos\vartheta \end{pmatrix}, \tag{5}$$

#150625 - $15.00 USD Received 6 Jul 2011; revised 2 Aug 2011; accepted 16 Aug 2011; published 23 Aug 2011

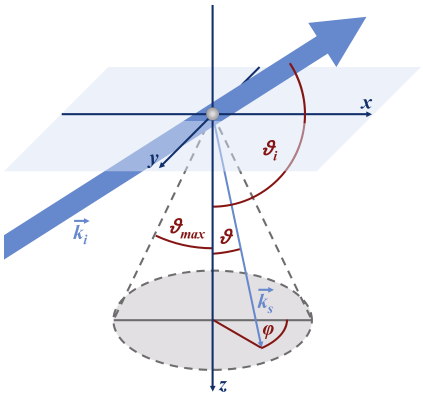

Fig. 1. Illustration of geometry and nomenclature which is used for the theoretical description of the scattering microscope.

where φ and ϑ is the azimuth angle and the polar angle of the scattered light, respectively. The polar angle of illumination is ϑ_i (see Fig. 1). The vectors $\vec{k}_i$ and $\vec{k}_s$ span a plane. For $\varphi = 0°$ or $\varphi = 180°$, this plane is equal to the plane spanned by the x- and the z-axis. Otherwise it is rotated by an angle ξ about the vector $\vec{k}_i$. Thus, their normal vectors $\vec{n}_{\varphi=0}$ and $\vec{n}(\varphi,\vartheta)$ are rotated in the same way,

$$\xi(\varphi,\vartheta) = \arccos\left(\vec{n}_{\varphi=0}\cdot\vec{n}(\varphi,\vartheta)\right). \tag{6}$$

In the case of unpolarized illumination, this does not have any effect. But in the case of (partly) linear polarized light, the polarization state is rotated too. This can be taken into account by the rotation matrix **R** [27]

$$\mathbf{R} = \begin{pmatrix} 1 & 0 & 0 & 0 \\ 0 & \cos(2\xi) & \sin(2\xi) & 0 \\ 0 & -\sin(2\xi) & \cos(2\xi) & 0 \\ 0 & 0 & 0 & 1 \end{pmatrix}. \tag{7}$$

In the experiment, polystyrene spheres are placed on top of a coverslip. The objective and the illumination are situated below this. Therefore, the incident beam and the light scattered by a sphere have to transmit the coverslip. Multiple reflections between its lower and upper interface are neglected in this theory due to the relatively weak effect on the result. The transmission matrix **T** is based on Fresnel's formulas [33]. For a single interface, it is

$$\mathbf{T} = \frac{1}{2}\begin{pmatrix} \tau_\perp+\tau_\parallel & \tau_\perp-\tau_\parallel & 0 & 0 \\ \tau_\perp-\tau_\parallel & \tau_\perp+\tau_\parallel & 0 & 0 \\ 0 & 0 & 2\sqrt{\tau_\perp\tau_\parallel} & 0 \\ 0 & 0 & 0 & 2\sqrt{\tau_\perp\tau_\parallel} \end{pmatrix}, \tag{8}$$

where $\tau_\perp$ and $\tau_\parallel$ are dependent on the angle of incidence α and the angle of refraction β

$$\tau_\perp = \left(\frac{\tan\alpha}{\tan\beta}\right)\left(\frac{2\sin\beta\cos\alpha}{\sin(\alpha+\beta)}\right)^2, \tag{9}$$

$$\tau_\parallel = \left(\frac{\tan\alpha}{\tan\beta}\right)\left(\frac{2\sin\beta\cos\alpha}{\sin(\alpha+\beta)\cos(\alpha-\beta)}\right)^2. \tag{10}$$

In case of a plan-parallel coverslip the transmission matrix has to be applied twice because of the two interfaces. The incident and the detected light is described by the Stokes vectors $\vec{S}_{in}$ and

#150625 - $15.00 USD Received 6 Jul 2011; revised 2 Aug 2011; accepted 16 Aug 2011; published 23 Aug 2011

$\vec{S}_{out}$, respectively. For the shown setup, it is

$$\begin{pmatrix} S_{out,0} \\ S_{out,1} \\ S_{out,2} \\ S_{out,3} \end{pmatrix} = \mathbf{T}^2_{\alpha=\vartheta} \cdot \mathbf{M} \cdot \mathbf{R} \cdot \mathbf{T}^2_{\alpha=180^\circ-\vartheta_i} \cdot \begin{pmatrix} S_{in,0} \\ S_{in,1} \\ S_{in,2} \\ S_{in,3} \end{pmatrix}. \tag{11}$$

In the experiment the incident light is unpolarized, thus its Stokes vector is $\vec{S}_{in} = \begin{pmatrix} 1 & 0 & 0 & 0 \end{pmatrix}^\top$. The detector is insensitive to polarization, therefore only the first element $S_{out,0}$ of $\vec{S}_{out}$ is of interest. Depending on the angle of illumination and the numerical aperture of the objective, the scattering microscope detects a range of polar angles $\vartheta = 0 \ldots \vartheta_{max}$ at once. The scattered light from all these angles is integrated and detected spectrally resolved. Therefore the theoretical scattering spectrum $I_T(\lambda, D)$ of a single sphere with diameter D measured by the scattering microscope is

$$I_T(\lambda, D) = \int_{\varphi=0}^{2\pi} \int_{\vartheta=0}^{\vartheta_{max}} S_{out,0}(\lambda, D, \varphi, \vartheta)\, r^2 \sin\vartheta \, \mathrm{d}\vartheta \mathrm{d}\varphi. \tag{12}$$

3. Materials and methods

The results are based on two different methods, particles in suspension measured by the collimated transmission and single particles measured by the scattering microscope. Hence, the following issues are presented separately for both methods: a detailed explanation of the setup, a short paragraph concerning the sample preparation, an instruction of the measurement procedure and, finally, a description of the raw data analysis.

3.1. Particles in suspension measured by the collimated transmission setup

3.1.1. Collimated transmission setup

As described before, with the collimated transmission setup, it is possible to measure the extinction coefficient μ_{ext} of semi-transparent fluids and solids. A scheme of the collimated transmission setup is shown in Fig. 2. A collimated light beam passes through the sample, in this case a filled cuvette, having a path length $d = 10\,\mathrm{mm}$ placed in an appropriate holder. The beam has a width of 3 mm, provided by a fiber based halogen lamp (HL-2000, OceanOptics, Dunedin, FL, USA) and a collimating lens. Parts of the light are scattered according to the scattering

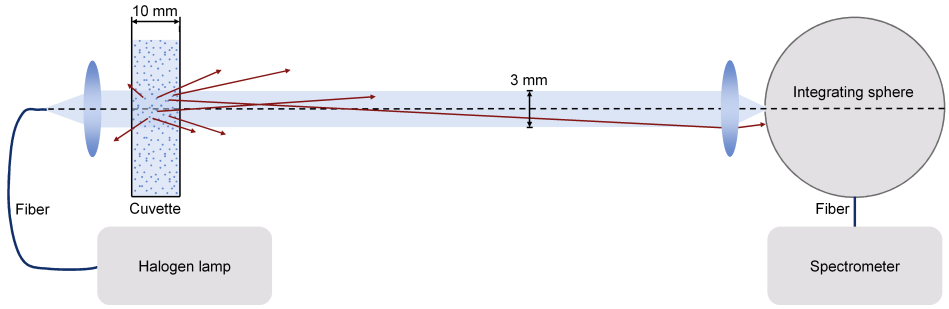

Fig. 2. Scheme of the collimated transmission setup. The scattered light is represented by red arrows.

#150625 - $15.00 USD Received 6 Jul 2011; revised 2 Aug 2011; accepted 16 Aug 2011; published 23 Aug 2011

coefficient of the suspension inside the cuvette which is related to the scattering cross sections of its included particles. In a relatively long distance behind the cuvette, here 45 cm, a lens focuses the unscattered light onto the small aperture of an integrating sphere. A spectrometer (USB2000, OceanOptics, Dunedin, FL, USA) is linked to the inner sphere surface via fiber optics. The complete setup is boxed, only the sample chamber is accessible for the operator. Therefore, it is very resistant and a suitable device for the comparison with other methods, e.g. the spectrally resolved scattering microscopy.

3.1.2. Sample preparation

Mie oscillations in the extinction spectrum are quenched, if the diameter distribution of the sphere suspension is too broad. The pattern of these oscillations ensures a high accuracy in the determination of this distribution. Therefore, monodisperse polystyrene particles having a relatively small size distribution are taken as samples (PS/Q-F-L1086, microparticles GmbH, Berlin, Germany). The particle size distribution is assumed by a Gaussian distribution, having a nominal mean diameter $\nu_n = 4.21\,\mu\text{m}$ and a nominal standard deviation $\sigma_n = 0.07\,\mu\text{m}$. This stock suspension is given in an ultrasonic bath for 30 minutes and afterwards a diluted intermediate stock is prepared. Its volume concentration should be high enough to measure a significant extinction, but low enough to avoid any side effects by multiple or dependent scattering. For this experiment a volume concentration $f_V \approx 10^{-4}$ is suitable.

3.1.3. Measurement procedure

First, a reference signal $I_0(\lambda)$ is taken by using a carefully cleaned cuvette filled with pure water to consider any reflections at the surface of the cuvette. Moreover, a dark spectrum $I_D(\lambda)$ is measured by closing the shutter of the lamp. Each measurement is performed with an integration time of 400 ms and averaged 10 times. The cuvette is filled with 1 ml of the intermediate stock. The transmitted intensity $I(\lambda)$ is measured multiple times to check for any temporal errors due to sinking particles or intensity fluctuations of the halogen bulb.

3.1.4. Data analysis

The light transmission $T(\lambda)$ is given by

$$T(\lambda) = \frac{I(\lambda) - I_D(\lambda)}{I_0(\lambda) - I_D(\lambda)}. \tag{13}$$

The extinction coefficient can be calculated by Lambert Beer's law. For non-absorbing suspensions $\mu_a(\lambda) = 0\,\text{cm}^{-1}$, it is equal to the scattering coefficient $\mu_s(\lambda)$

$$\mu_{ext,E}(\lambda) = \mu_s(\lambda) + \mu_a(\lambda) = -\frac{\log T(\lambda)}{c\,d} \tag{14}$$

the concentration of the intermediate stock solution is defined as $c = 1$. This experimental result is compared to theoretical calculations using Eq. 2. Therefore a set of Gaussian distributions $g(D)$ is created having different mean values $\nu = 4 \ldots 4.5\,\mu\text{m}$ ($\Delta\nu = 0.1\,\text{nm}$) and standard deviations $\sigma = 0 \ldots 100\,\text{nm}$ ($\Delta\sigma = 0.1\,\text{nm}$). With this, a set of theoretical extinction curves $\mu_{ext,T}(\lambda, \nu, \sigma)$ is created and divided by the experimental extinction curve $\mu_{ext,E}(\lambda)$

$$V(\lambda, \nu, \sigma) = \frac{\mu_{ext,T}(\lambda, \nu, \sigma)}{\mu_{ext,E}(\lambda)}. \tag{15}$$

In case of perfect agreement between theoretical and experimental extinction, this function $V(\lambda, \nu, \sigma)$ is a straight curve versus λ without any oscillating parts. The harmonic content F is

#150625 - $15.00 USD Received 6 Jul 2011; revised 2 Aug 2011; accepted 16 Aug 2011; published 23 Aug 2011

defined by

$$F(\nu,\sigma)=\frac{\sqrt{\sum_{\lambda=\lambda_s}^{\lambda_e}\left(V(\lambda,\nu,\sigma)-\overline{V}(\nu,\sigma)\right)^2}}{\sqrt{\sum_{\lambda=\lambda_s}^{\lambda_e}V^2(\lambda,\nu,\sigma)}}, \tag{16}$$

with the wavelengths $\lambda_s = 450\,\text{nm}$ and $\lambda_e = 800\,\text{nm}$. $\overline{V}(\nu,\sigma)$ is the mean value of $V(\lambda,\nu,\sigma)$ over λ. The global minimum of this function $F(\nu,\sigma)$ determines the corresponding parameters ν_{CT} and σ_{CT} having the best agreement between experiment and theory. The calculation of the scattering cross sections $C_s(\lambda,D)$ is time consuming, but has to be done only once. The second part of the algorithm is fast and therefore suitable for the analysis of large numbers of experimental data.

3.2. Single particles measured by the spectrally resolved scattering microscope

3.2.1. Scattering microscope setup

The scattering microscope enables the measurement of scattered light by single particles. Its setup was developed in a way that both, spectrally and angular resolved measurements, are possible. However, only the part of the spectrally resolved setup is explained herein. The setup is based on an inverted microscope (see Fig. 3). A reflected darkfield illumination is realized by a collimated beam that is provided by a supercontinuum laser source (SuperK Blue, NKT Photonics A/S, Birkerød, Denmark). Therefore, integration times below 100 ms are possible. As shown in earlier works [34], a common broadband source can also be used, with the main drawback of much longer integration times. The angle of illumination $\vartheta_i = 124^\circ$ is not in

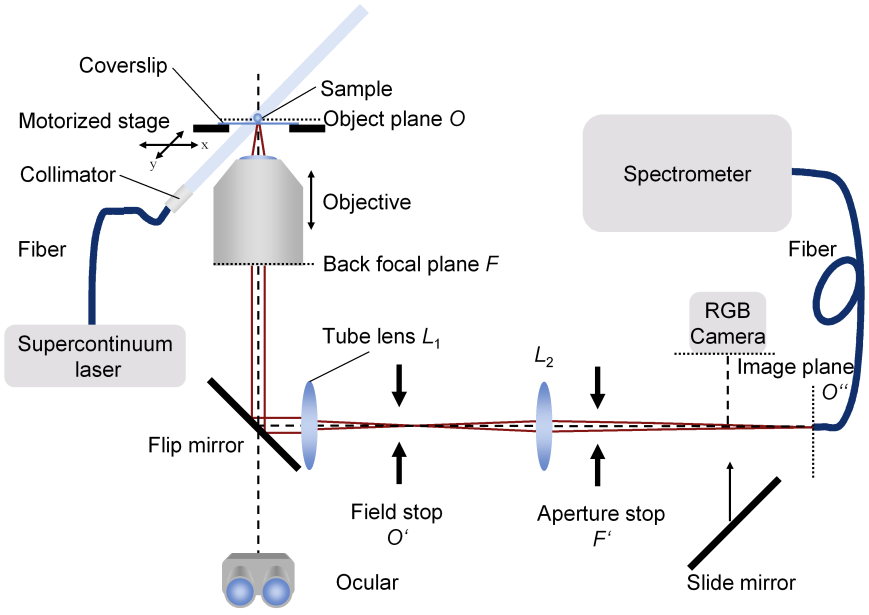

Fig. 3. Scheme of the scattering microscope. Only the path of the spectrally resolved measurement method is presented. The scattered light is represented by red solid lines. The optical axis is drawn with black dashed lines.

#150625 - $15.00 USD Received 6 Jul 2011; revised 2 Aug 2011; accepted 16 Aug 2011; published 23 Aug 2011

the detectable range of the objective $\vartheta_{max} = 9.2^\circ$ which is given by the numerical aperture $NA = 0.16$ (EC Plan-Neofluar 5x/0.16, Carl Zeiss AG, Oberkochen, Germany). Thus, no reflected light by the coverslip but only scattered light by the sample can be detected by the objective. The front focal plane of the tube lens L_1 ($f_1 = 160\,\mathrm{mm}$) is situated in the back focal plane F of the objective. An iris is placed in the first intermediate image O' which is equal to the back focal plane of the tube lens L_1. Another lens L_2 ($f_2 = 100\,\mathrm{mm}$) is placed 300 mm behind the tube lens L_1. Therefore an intermediate plane F' of the Fourier plane can be found in its back focal plane and an image plane O'' can be found 490 mm behind the first intermediate image O'. In this plane one end of a glass fiber with a core diameter of 1000 µm is positioned. The other end is connected to a CCD spectrometer (MCS-CCD-Lab, Carl Zeiss AG, Oberkochen, Germany). Alternatively, a mirror can be slid into the optical path, so instead of the fiber a camera with RGB sensor (NS1300CU, NET GmbH, Finning, Germany) acquires the object in the image plane O''. The overall magnification is given by the objective, the focal length f_1 of the tube lens L_1, the position and the focal length f_2 of lens L_2. Hence, the calculated overall magnification is 12.5. The imaging resolution of the setup is limited due to the low numerical aperture of the objective (working distance 18.5 mm) but is still good enough to align samples as single polystyrene spheres or cells and cell cores. In case of spectrally resolved scattering microscopy, the small NA is an advantage as the integration over a small range of scattering angles does not cancel spectral oscillations and thus information content is preserved.

3.2.2. Sample preparation

Exactly the same stock suspension which is measured by the collimated transmission setup is reused for the single particle samples. Therefore, the suspension is diluted again by a factor of 10 with pure water and homogenized in an ultrasonic bath. Afterwards a drop of this suspension having a volume of 20 µl is placed on a coverslip. This sample is air-dried in a clean box to protect it from disturbing dust particles.

3.2.3. Measurement procedure

The coverslips are placed – with the polystyrenes on top – onto the microscope stage. Thus, forward scattered light by a particle – which is in general much stronger than backscattered light – is not reflected at the coverslip and therefore not detected by the objective. The selection of suitable single particles is done manually and randomly by the operator with help of the motorized stage and the camera (see Fig. 4). The only restriction is the minimum distance of 80 µm to the nearest particle which is dependent on the core diameter of the fiber and the overall

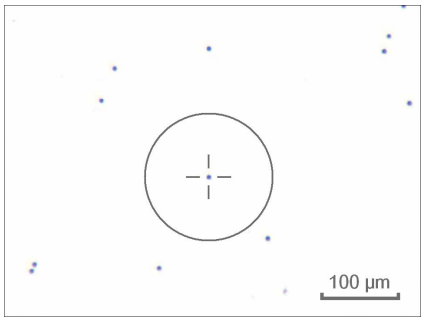

Fig. 4. Brightfield image of air-dried polystyrene spheres taken by the camera. The reticule marks the corresponding central position of the fiber in the image plane. The circle represents the required minimum distance of 80 µm to the next nearest particle.

#150625 - $15.00 USD Received 6 Jul 2011; revised 2 Aug 2011; accepted 16 Aug 2011; published 23 Aug 2011

magnification of the system. Sufficient particles are measured separately to obtain a significant statistic. Moreover, for each particle, the spectrum of a spot nearby is measured to subtract the background signal of scattered light caused by the coverslip. A reference signal, obtained by the measurement of a reflection standard, was not taken because it is not implicitly needed for the following analysis.

3.2.4. Data analysis

The analysis of the spectra is automated by a self-written MATLAB code to achieve fast, reproducible and objective results [34]. A set of theoretical spectra $I_T(\lambda, D)$ with varying particle diameters $D = 3 \ldots 5.5\,\mu\text{m}$ ($\Delta D = 1\,\text{nm}$) is calculated in advance as shown in section 2.2. Each experimental spectrum $I_{E,n}(\lambda)$ is compared to this set (n is the number of sphere).

The experimental $I_{E,n}(\lambda)$ and the theoretical spectra $I_T(\lambda, D)$, are differentiated. The correlation $C_n(D)$ of these derivatives is calculated for wavelengths in the range between $\lambda_s = 450\,\text{nm}$ and $\lambda_e = 800\,\text{nm}$

$$C_n(D) = \sum_{\lambda=\lambda_s}^{\lambda_e} \frac{\mathrm{d}I_{E,n}(\lambda)}{\mathrm{d}\lambda} \cdot \frac{\mathrm{d}I_T(\lambda, D)}{\mathrm{d}\lambda}. \tag{17}$$

The corresponding diameters of the theoretical spectra with the maximum correlation of $C_n(D)$ are termed D_n.

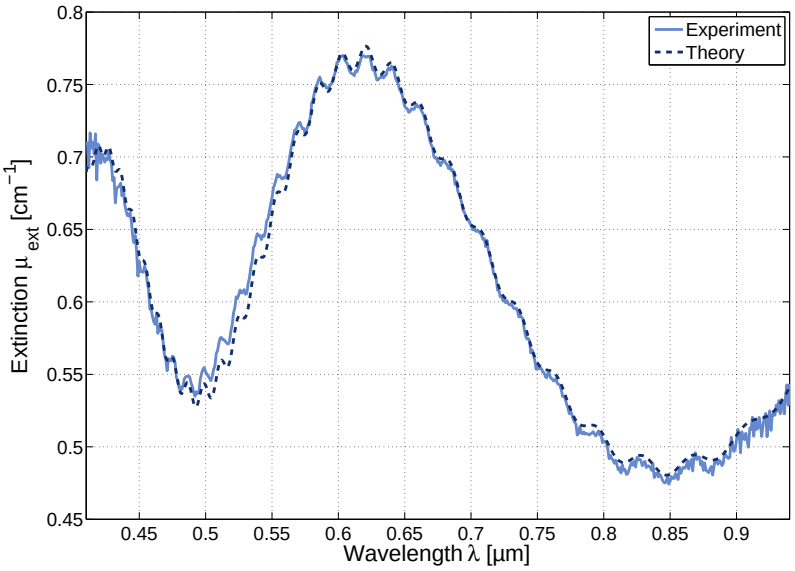

Fig. 5. Extinction spectrum $\mu_{ext,E}(\lambda)$ of a polystyrene bead suspension measured by the collimated transmission setup (light blue solid line). Additionally, the theoretical curve $\mu_{ext,T}(\lambda, v_{CT}, \sigma_{CT})$ with $v_{CT} = 4.1468\,\mu\text{m}$ and $\sigma_{CT} = 0.0208\,\mu\text{m}$ is shown (dark blue dashed line).

#150625 - $15.00 USD Received 6 Jul 2011; revised 2 Aug 2011; accepted 16 Aug 2011; published 23 Aug 2011

4. Results and discussion

4.1. Particles in suspension measured by the collimated transmission setup

Suspensions from the intermediate stock were measured three times by the collimated transmission setup as explained in section 3.1.3. The mean value $v_{CT} = 4.1468 \pm 0.0007\,\mu\text{m}$ and the standard deviation $\sigma_{CT} = 0.0208 \pm 0.0004\,\mu\text{m}$ of an assumed Gaussian size distribution were obtained with the self-written algorithm explained in section 3.1.4. Figure 5 presents the experimentally measured extinction spectra averaged over all three measurements. Below 450 nm and above 800 nm, the signal to noise ratio of the spectrum is decreasing due to lack of light intensity and detector sensitivity. Moreover, the corresponding theoretical curve is plotted in dashed lines. Both curves are in very good agreement to each other. The largest deviations can be found between 500 nm and 550 nm, with relative differences smaller than 3 %.

4.2. Single particles measured by the spectrally resolved scattering microscope

In total, 150 single polystyrene beads were measured by the spectrally resolved scattering microscope. All spectra were analyzed by the self-written correlation algorithm. The solid line in Fig. 6 represents a typical experimental spectrum of a single polystyrene bead (number $n = 121$ of 150). In addition, the corresponding theoretical curve obtained by the correlation algorithm is plotted. In this case the experimentally identified diameter is $D_{121} = 4.145\,\mu\text{m}$. The experimental curve was referenced by a tenth-order polynomial and normalized onto the theoretical curve. The intensity values of the characteristic Mie oscillations show some discrepancies. However, very good agreement can be found for the spectral positions of the Mie oscillations which is important for a correct size determination of the sphere. Figure 7 gives a section of the corresponding correlation functions $C(D)$ of the experimental and the theoretical curve shown in

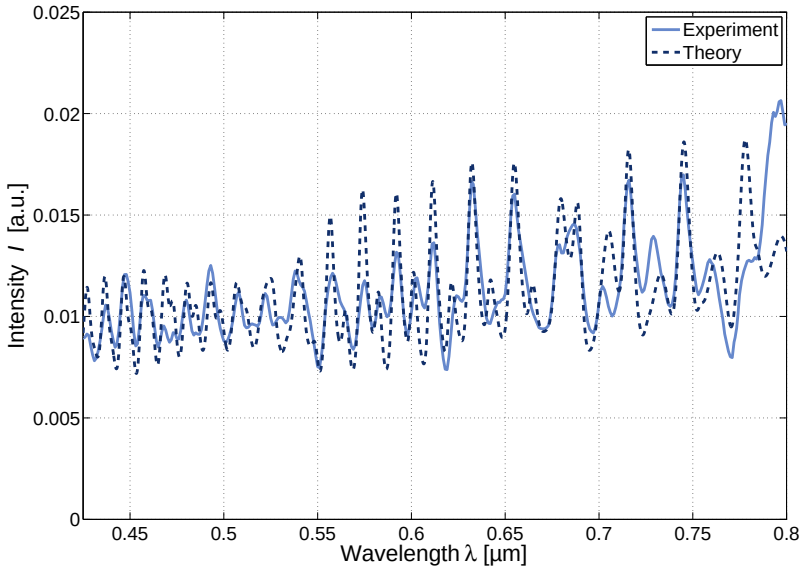

Fig. 6. Spectrum $I_{E,121}(\lambda)$ of a single polystyrene sphere measured by the scattering microscope (light blue solid line). Additionally, the theoretical curve $I_T(\lambda, D_{121})$ with $D_{121} = 4.145\,\mu\text{m}$ is shown (dark blue dashed line). The experimental spectrum $I_{E,121}(\lambda)$ is scaled onto the theoretical values $I_T(\lambda, D_{121})$.

#150625 - $15.00 USD Received 6 Jul 2011; revised 2 Aug 2011; accepted 16 Aug 2011; published 23 Aug 2011

Fig. 6. The global maximum of both curves is at $D_{121} = 4.145\,\mu\text{m}$. The full width at half maximum of the main lobe is 27 nm for the experimental and 24 nm for the theoretical spectrum, respectively. Therefore, the experimentally determined size resolution is very close to the best possible value that is given by the theory for this setup.

The diameters D_n of all 150 spheres are plotted in a histogram (see Fig. 8). Their mean diameter is $v_{SM} = 4.1442\,\mu\text{m}$ and the standard deviation is $\sigma_{SM} = 0.0269\,\mu\text{m}$. In comparison, the Gaussian distribution obtained by the collimated transmission setup is plotted as well ($v_{CT} = 4.1468\,\mu\text{m}$ and $\sigma_{CT} = 0.0208\,\mu\text{m}$). The difference of both methods in mean diameter and standard deviation are 2.6 nm and 6.1 nm, respectively.

In test measurements, the statistical error $\Delta D = 2.3\,\text{nm}$ was determined by measuring the diameter D of an identical particle several times. Deviations are caused by imperfect centering of a polystyrene sphere in the x-y-direction and varying focal planes of the objective. It is assumed that every diameter D_n is measured with the same statistical error $\Delta D_n = \Delta D$. Hence, by applying the law of error propagation, the statistical error of the calculated mean diameter v_{SM} can be derived as

$$\Delta v_{SM} = \sqrt{\sum_{m=1}^{N} \left[\frac{\partial}{\partial D_m} \frac{1}{N} \sum_{n=1}^{N} D_n \right]^2 (\Delta D)^2} = \frac{\Delta D}{\sqrt{N}}. \tag{18}$$

The statistical error of the standard deviation σ_{SM} is analogously given by

$$\Delta \sigma_{SM} = \sqrt{\sum_{m=1}^{N} \left[\frac{\partial}{\partial D_m} \left(\frac{1}{N-1} \sum_{n=1}^{N} (D_n - v_{SM})^2 \right)^{0.5} \right]^2 (\Delta D)^2} = \frac{\Delta D}{\sqrt{N-1}}. \tag{19}$$

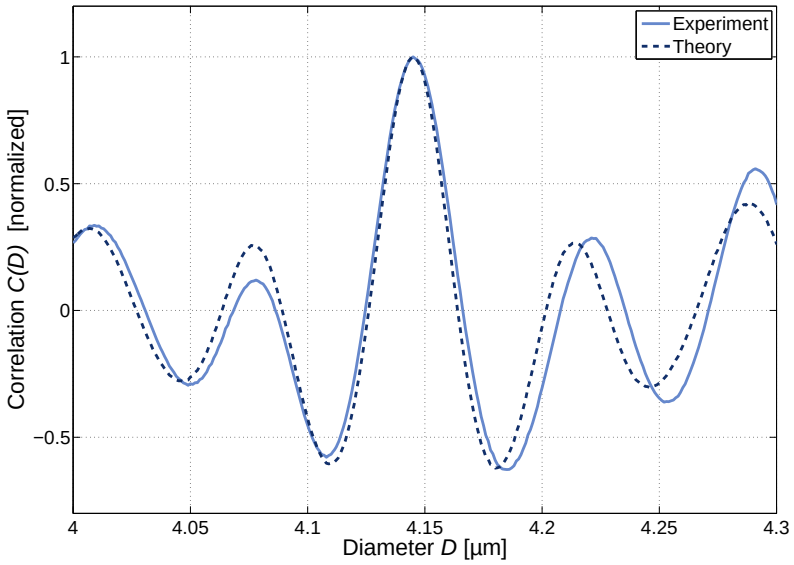

Fig. 7. Normalized correlation function $C(D)$ of the measured spectrum $I_{E,121}(\lambda)$ from Fig. 6 (light blue solid line). Its global maximum is at $D_{121} = 4.145\,\mu\text{m}$. Additionally, a theoretical correlation function is plotted as well (dark blue dashed line). It was calculated for the corresponding theoretical spectrum $I_T(\lambda, D_{121})$.

#150625 - $15.00 USD Received 6 Jul 2011; revised 2 Aug 2011; accepted 16 Aug 2011; published 23 Aug 2011

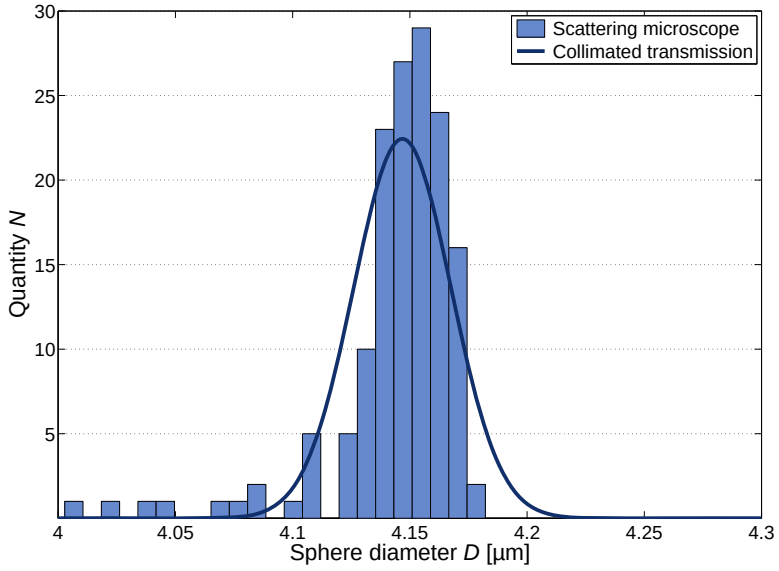

Fig. 8. Histogram of 150 sphere diameters D_n which were determined separately by spectrally resolved scattering microscopy (mean value $v_{SM} = 4.1442\,\mu m$ and standard deviation $\sigma_{SM} = 0.0269\,\mu m$). The solid line represents a Gaussian size distribution determined by collimated transmission measurements of polystyrene bead suspensions (mean value $v_{CT} = 4.1468\,\mu m$ and standard deviation $\sigma_{CT} = 0.0208\,\mu m$)

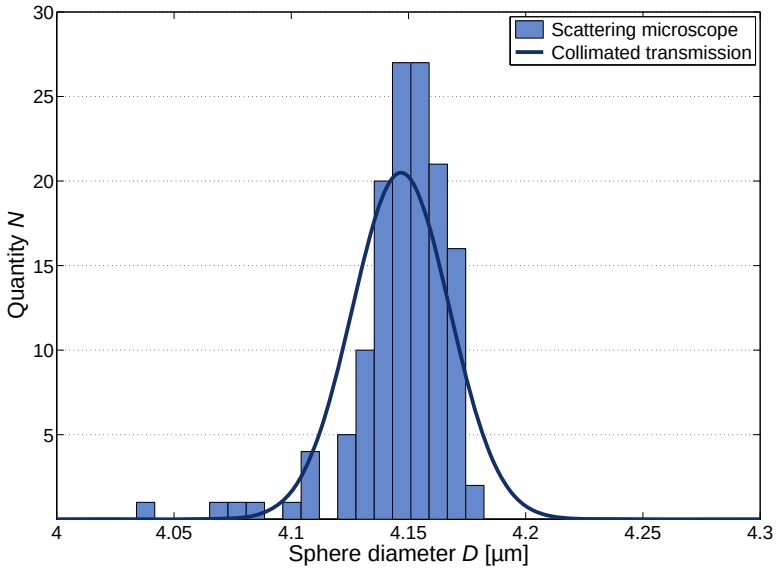

.

Fig. 9. Modified histogram from Fig. 8 considering the threshold C_{min}. The mean diameter and the standard deviation of the remaining 137 spheres is $v'_{SM} = 4.1471\,\mu m$ and $\sigma'_{SM} = 0.0206\,\mu m$, respectively.

#150625 - $15.00 USD Received 6 Jul 2011; revised 2 Aug 2011; accepted 16 Aug 2011; published 23 Aug 2011

Due to the large number of measurements ($N = 150$), the statistical error of mean diameter ν_{SM} and standard deviation σ_{SM} is $\Delta\nu_{SM} = 0.2\,\text{nm}$ and $\Delta\sigma_{SM} = 0.2\,\text{nm}$, respectively.

Therefore, the results of both measurements show deviations in mean diameter and standard deviation that are larger than the statistical errors . Moreover, the size distribution of the single spheres differs from a Gaussian shape. Especially, the relatively large amount of spheres having a diameter D_n smaller than $\nu_{SM} - 3 \cdot \sigma_{SM} = 4.0635\,\mu\text{m}$ is noticeable. Their corresponding experimentally measured spectra $I_{E,n}(\lambda)$ show relatively weak correlations $C_n(D_n)$ with the theoretically calculated spectra $I_T(\lambda, D_n)$. A threshold C_{min} guarantees that only spectra with a sufficiently good correlation are taken into account and ensures an analysis on well-approved data. This threshold C_{min} was calculated by the mean value ν_C and the standard deviation σ_C of all 150 correlation values $C_n(D_n)$

$$C_{min} = \nu_C - \sigma_C. \tag{20}$$

Considering the threshold C_{min}, 137 out of 150 spectra remained, the diameters D_n of these are plotted in a second histogram (see Fig. 9). For these, the mean diameter is $\nu'_{SM} = 4.1471 \pm 0.0002\,\mu\text{m}$ and the standard deviation is $\sigma'_{SM} = 0.0206 \pm 0.0002\,\mu\text{m}$. It still does not have a perfect Gaussian shape, but it is similar enough. Therefore it is proper to analyze the collimated transmission measurements in Fig. 5 with the assumption of a Gaussian size distribution. Mean value and standard deviation of both methods differ by $0.3\,\text{nm}$ and $0.2\,\text{nm}$, respectively, which is in agreement within the measurement accuracy.

5. Conclusion

A novel setup of a spectrally resolved scattering microscope was presented in detail and evaluated by comparing results with a well-approved second setup, the collimated transmission. Both methods are based on spectrally resolved elastic light scattering. Diameters of polystyrene beads were determined by the analysis of the spectrally resolved scattering pattern using Mie theory. Hence, the size distribution was determined for both methods. The results are in excellent agreement, the systematic error of the mean diameters and standard deviations is $0.3\,\text{nm}$ and $0.2\,\text{nm}$, respectively , which is within the measurement accuracy (outliers are neglected).

In comparison, other validations of spectroscopic light scattering experiments which can be found in literature show deviations in the range of several nanometers [10, 17], although similar sphere suspensions were used. Further, the nominal values given by the manufacturer ($\nu_n = 4.21\,\mu\text{m}$ and $\sigma_n = 0.07\,\mu\text{m}$) differ by more than $50\,\text{nm}$. Besides, the resulting histogram from Fig. 8 includes additional information about the mismatch between the assumed and the actual size distribution, which is rarely published by the manufacturers.

It should be kept in mind that for a single measurement the statistical error of both methods depends on the size of the particles and can be in the range of a few nanometer. Nevertheless, this is still a remarkable resolution with errors in the per mil range. Thus, scattering microscopy should not only be able to detect diameters within a few nanometers of different spheres [35] but also temporal changes of one and the same particle or sample [36]. This feature might be used e.g. to observe the growth of neoplastic cells [20] or to monitor the apoptosis of living cells [37]. The non-spherical shape of cells and the lower differences in the refractive indices are going to be new challenges in future work.

As mentioned before the scattering microscope is suitable for angular resolved measurements, too. Details on that part are going to be published in a separate contribution.

Acknowledgments

This work was financed by the Baden-Württemberg Stiftung gGmbH and the Deutsche Forschungsgemeinschaft (DFG).

#150625 - $15.00 USD Received 6 Jul 2011; revised 2 Aug 2011; accepted 16 Aug 2011; published 23 Aug 2011